JOURNAL OF APPLIED ELECTROCHEMISTRY 23 (1993) 1151–1161

A modelling approach to the optimizaton of lead–acid battery electrodes

G. MAIA, E. A. TICIANELLI, E. R. GONZALEZ

Instituto de Física e Química de São Carlos – USP, C. P. 369, 13560 São Carlos, SP. Brazil

Received 18 August 1992; revised 1 February 1993

A resistive grid model was used to study the current and ohmic overpotential distributions along the surface of lead–acid battery electrodes. Analyses were made under two different regimes: the initial behaviour at high current densities and the response with time at low current densities. At high discharge currents the theoretical results show that the geometry of the electrodes and the position of the lug play the most important role in controlling the magnitude of ohmic losses. The best geometry is a square grid with the lug positioned at the upper centre of the electrode. At low discharge currents the model was used to follow the current distribution along the electrode surface as a function of time. In this last study the appearance, for long discharge times, of short-circuited concentration microcells localized in certain regions of the electrode surface was noted. The other regions of the electrode supply the external discharge current and the excess current necessary to charge the internal microcell.

1. Introduction

One of the most widely used experimental methods for the characterization of lead–acid batteries is the recording of charge/discharge–time curves. Although useful practical information, particularly comparative, can be derived from these measurements they can not be quantitatively correlated with the local parameters that describe the phenomena taking place in the electrode materials and the electrolyte. Because of this, there has been great interest in developing theoretical models that can be treated mathematically with the purpose of reproducing the response of the whole system from the predicted behaviour of local values [1–24]. In conjunction with selected experimental measurements, modelling can reduce considerably the time and investment needed to obtain the desired results.

Two main basic approaches have been used for the mathematical description of the system: the macrohomogeneous model [1–15] and the resistive grid model [16–24]. In the first case, the electrode process is treated in terms of the kinetics and mechanism of the electrochemical reactions taking place in an electrolyte flooded porous structure. Current density and overpotential relationships are obtained as a function of pore size distribution, the electronic conductivity of the porous structure, the electrolyte conductivity inside the porous matrix and the transport properties of active reactants. In the resistive grid model actual size battery electrodes are divided into a discrete number of elements with independent physical and electrochemical properties. One element in the positive plate and the counterpart in the negative electrode, together with the electrolyte and separator between them, form an individual microcell whose electrochemical properties can be determined independently as a function of the state of discharge and electrolyte composition. Current and overpotential distributions along the electrode surface are obtained connecting the elements in an electrical circuit, equivalent to a resistive grid network, and applying the Ohm and Kirchoff laws.

Due to the complexity of the modelling processes it is customary to introduce simplifying assumptions that necessarily limit the validity of the final results. Recently, Morimoto *et al.* [23] pointed out the limitations of previous treatments and reported interesting results using a less restrictive resistive grid model complemented with some simple experimental measurements. They were able to obtain the potential and current distributions on the electrodes which makes it possible, in principle, to predict the performance of any cell design.

In view of these results, it was considered worthwhile to use the model presented by Morimoto *et al.* [23] to analyze lead–acid cells with different electrode dimensions, grid configurations and lug size and position in order to predict the best geometry for the system and also to gain a deeper understanding of the problem of stratification of the electrolyte.

2. Theoretical model

Although described in the literature the essential aspects of the model of Morimoto *et al.* [23] will be presented for consistency. The diagram of Fig. 1 shows a set of positive and negative electrodes and illustrates the coordinate system used in the model. The analysis is made in terms of J, the current density between the electrodes and i_{px}, i_{py}, i_{nx} and i_{ny}, the linear current densities (current per unit width)

0021-891X

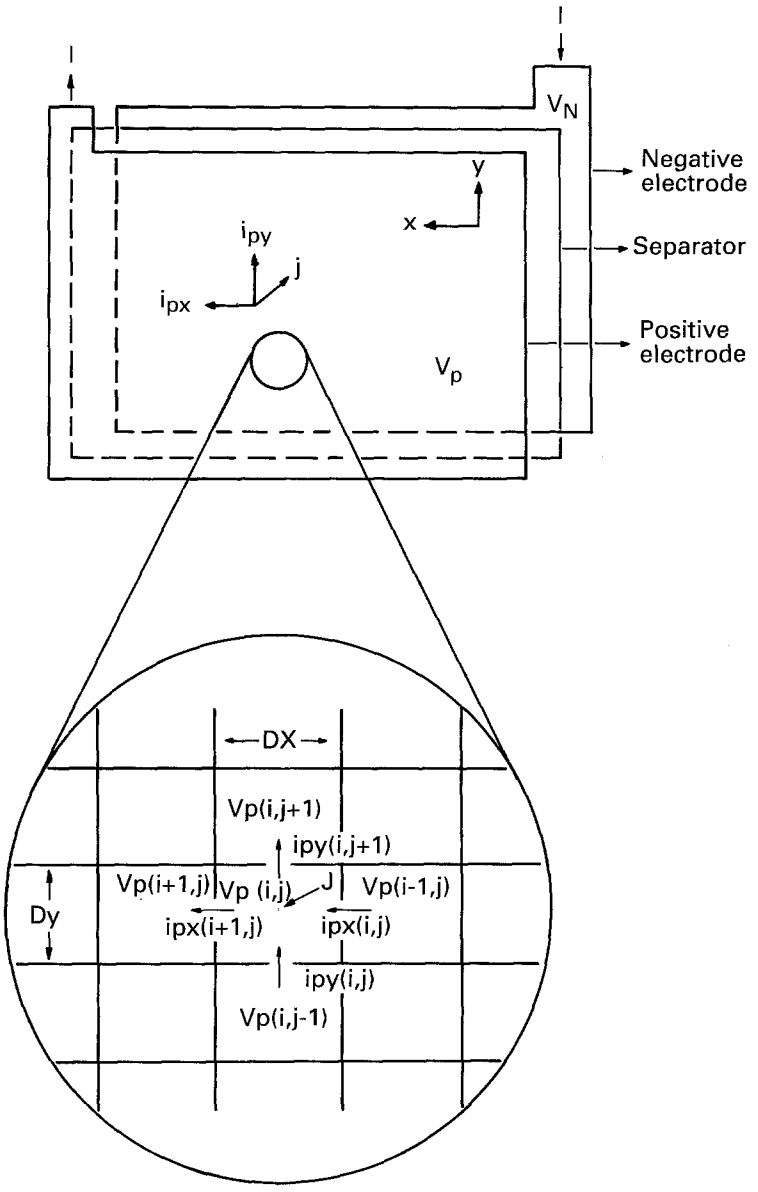

Fig. 1. Diagram of a lead–acid cell, illustrating the coordinate system and the discretization used in the finite difference method.

within the positive and negative plates. To solve the differential equations arising from the application of Ohm and Kirchoff laws to the cell in Fig. 1 a finite difference method, also illustrated in Fig. 1, is used. In the present case the final equations are [23]:

$$\left.\begin{aligned} &\frac{i_{px}(i+1,j)-i_{px}(i,j)}{\Delta_x} \\ &\quad+\frac{i_{py}(i,j+1)-i_{py}(i,j)}{\Delta_y} \\ &\quad-J(i,j)=0 \\ &\frac{i_{nx}(i+1,j)-i_{nx}(i,j)}{\Delta_x} \\ &\quad+\frac{i_{ny}(i,j+1)-i_{ny}(i,j)}{\Delta_y} \\ &\quad+J(i,j)=0 \end{aligned}\right\} \quad (1)$$

$$\left.\begin{aligned} i_{px}&=\frac{-2[V_p(i,j)-V_p(i-1,j)]}{[r_p(i,j)+r_p(i-1,j)]\Delta x} \\ i_{py}&=\frac{-2[V_p(i,j)-V_p(i,j-1)]}{[r_p(i,j)+r_p(i,j-1)\Delta y} \\ i_{nx}&=\frac{-2[V_n(i,j)-V_n(i-1,j)]}{[r_n(i,j)+r_n(i-1,j)]\Delta x} \\ i_{ny}&=\frac{-2[V_n(i,j)-V_n(i,j-1)]}{[r_n(i,j)+r_n(i,j-1)]\Delta y} \end{aligned}\right\} \quad (2)$$

where $V_p(i,j)$ and $V_n(i,j)$ are the potentials and $r_p(i,j)$ and $r_n(i,j)$ are the effective resistances (see below) of the positive and negative electrodes, respectively.

The equation correlating $J(i,j)$ with $V_p(i,j)$ and $V_n(i,j)$ is obtained from experimental polarization data using small electrodes (see below) and

an n-order polynomial of the form:

$$J(i,j) = a(0) + a(1)(V_p(i,j) - V_n(i,j)) + \ldots + a(n)[V_p(i,j) - V_n(i,j)]^n \quad (3)$$

When a $A \times B$ grid mesh is used for electrode mapping, substitution of Equations 2 and 3 into Equation 1 gives $2 \times A \times B$ non linear equations expressed in terms of $V_p(i,j)$, $V_n(i,j)$, $r_p(i,j)$, $r_n(i,j)$, Δx and Δy.

2.1. *Boundary conditions*

On the edge of the electrode, the current component normal to the edge is zero except on the lug. In the finite difference approach this means that $V(L,j) = V(M,j)$, where L is the last i segment (left and right) inside the plate and M the corresponding neighbour outside the plate. A similar reasoning can be applied to the upper and lower edges.

For a constant discharge current (I_0), the terminal voltage on the lug in the positive plate (V_p) is related to I_0 through the expression:

$$\sum_{i=0}^{W} \frac{2(V_p - V_p)(i,T))}{(r_p + r_p(i,T))\Delta y} = \frac{I_0}{\Delta x} \quad (4)$$

where $w = W/\Delta x$ (W = lug width), $V_p(i,T)$ and $r_p(i,T)$ are the voltage and resistance of the top finite elements, respectively, and r_p is the sheet resistance of the lug material (see below). The negative plate was treated in a similar way. For the purpose of performing calculations the terminal voltage of the lug of the negative plate (V_n) can be set equal to zero.

2.2. *Resistances of the plates*

The sheet resistances $r_p(i,j)$ and $r_n(i,j)$ are the average resistances per unit length of unit width of the segments of the positive and negative plates, respectively, and are given by:

$$\left.\begin{aligned} r_p(i,j) &= 1/\sigma_p(i,j)\,t_p \\ r_n(i,j) &= 1/\sigma_n(i,j)\,t_n \end{aligned}\right\} \quad (5)$$

where $\sigma_p(i,j)$ and $\sigma_n(i,j)$ are the specific conductances of the positive and negative plates and t_p and t_n the corresponding thicknesses.

3. Experimental details

Several kinds of experiments were performed to solve the mathematical model [23]. These include the following determinations:

(i) The electrode potential–current density relationship for different microcells with the positive and the negative electrodes in several states of discharge and electrolyte concentration. The cell voltage–current density characteristics can be obtained combining the above measurements and incorporating the ohmic loss due to the electrolyte and separator in the real cell.

(ii) The electrolyte concentration (density) between the electrodes for different segments in the real cell in several states of discharge.

(iii) The values of r_p and r_n are calculated from the experimentally measured conductivities of the grid and active materials. For this purpose the electrode plate is assumed to be composed of a flat sheet of the grid material over which a uniform layer of the active paste is deposited. The thicknesses of the grid material and the paste layers are calculated as one half of the total volume measured for each material divided by the electrode area. The presence of diagonal elements in the grid is considered by increasing the sheet thickness in the corresponding spatial domain.

The main characteristics of the electrodes used in the experimental part of this work were as follows:

1/2 Thickness of the positive grid	0.019 cm
1/2 Thickness of the negative grid	0.020 cm
1/2 Thickness of the active positive material	0.067 cm
1/2 Thickness of the active negative material	0.065 cm
Conductivity of the metallic grid	3.386×10^4 S cm^{-1}
Conductivity of the active positive material	1.727×10^2 S cm^{-1}
Conductivity of the active negative material	1.815×10^3 S cm^{-1}
Resistance of the positive electrode	1.558×10^{-3} Ω
Resistance of the negative electrode	1.266×10^{-3} Ω
Resistance of the lugs	1.790×10^{-4} Ω

The values of the conductivities are of the same order of magnitude as those reported in the literature [19, 20, 23] for both positive and negative materials.

Figure 2 illustrates the dimensional details of the grid used in the plates. A particular aspect to be noted is the presence of distributed diagonal elements. Each electrode, positive and negative, was divided into a 10 (x-axis) by 20 (y-axis) mesh grid. The resulting 400 nonlinear equations were solved, taking into account the boundary conditions, using the Powell hybrid method which is a modification of the Newton-Raphson classical method [25–27]. Computational routines were implemented from the NAG Fortran Library (Mark 13), The Numerical Group Ltd., Oxford (1988).

The simulation of the discharge of the electrodes was done at high and low current densities. In each case, particular experimental results were needed.

3.1. *High current densities*

Overpotential and current distributions over the electrode surfaces were determined for a current density

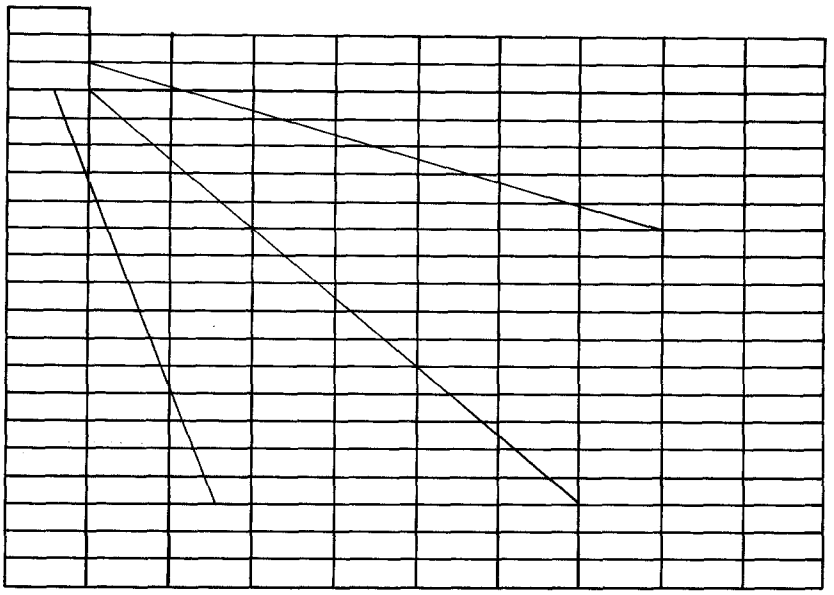

Fig. 2. Characteristics of the grid of the electrodes used to obtain the experimental results: width 14.45 cm, height 9.7 cm, lug width 1.2 cm and lug height 1.0 cm. The lug is in the left (right) upper corner of the positive (negative) electrode.

of 300 mA cm^{-2} under conditions of full charge. This corresponds to a practical situation in which the electrolyte (H_2SO_4 solution) density is 1.270 g cm^{-3}, $r_p(i,j) = 1.56 \times 10^{-3}\,\Omega$, $r_n(i,j) = 1.27 \times 10^{-3}\,\Omega$, $r(\text{lug}) = 1.79 \times 10^{-4}\,\Omega$ and $I_0 = 42.05$ A. The values of the resistances were calculated from conductivity data obtained for the materials of the grid and active paste using a four probe method.

Experimental data of $J(i,j)$ against $[V_p(i,j) - V_n(i,j)]$ were obtained through polarization measurements using 0.64 cm^2 samples of negative and positive electrodes in a conventional half-cell setup containing H_2SO_4 solution ($d = 1.270$ g cm^{-3}). An excess of electrolyte was present in order to avoid concentration changes. The auxiliary electrodes were large area (20 cm^2) lead foils positioned parallel to both faces of the working electrode. Potentials were measured using a reversible hydrogen reference electrode.

Measurements were made by applying a constant current in the range 0–200 mA cm^{-2} and recording the steady state potential. To prevent changes in the state of discharge the working electrode was recharged back to the initial state after each current step. The resistance of the electrolyte was measured using a general method [28] and the value obtained was 0.121 $\Omega\,cm^2$. This was used to evaluate the ohmic drop at each current density.

3.2. *Low current densities*

In the low current density regimes the objective was to evaluate the effect of time, and the consequent stratification of the electrolyte, on the current and potential distributions.

The electrolyte density was mapped experimentally, for different discharge states, using a complete cell consisting of five positive and six negative electrodes discharging at 5 mA cm^{-2} for 7 h. Interplate spacing was 2 mm and top, bottom and sides of the plates were at 1 cm from the container vessel walls. Samples of the electrolyte were collected through capillary glass tubing placed at various vertical positions between the separator and the positive electrode. Densities were taken as the mean value of four independent experiments. Standard deviation of the data were ± 0.005 g cm^{-3}.

The polarization characteristics at each point on the electrodes were obtained experimentally, using the same setup and procedure described above, for samples with states of discharge of 0, 25, 50 and 75% and for electrolyte densities of 1.10, 1.15, 1.20, 1.25 and 1.30 g cm^{-3}.

4. Results and discussion

4.1. *High discharge currents*

The main objective of the theoretical analyses made for high discharge currents is to establish the magnitude of ohmic losses and the current density distribution on the electrodes of a lead–acid battery. As explained above, the dependence of the potential difference with the current density was determined experimentally and the results, corrected for ohmic drop, are presented in Fig. 3. Values from this curve needed in the simulation, for current densities up to 350 mA cm^{-2}, were obtained by either interpolation or extrapolation after fitting the experimental data with a 3rd order polynomial (cf. Equation 3).

The high current analyses were made for several electrode dimensions, grid configurations and lug size and position in order to determine the effect of different geometries on ohmic losses. The following situations were considered:

Case 1: Grid size of width 14.45 cm and height 9.7 cm; lug size of width 1.2 cm and height 1.0 cm. Lug position: left upper corner of the positive electrode and right upper corner of the negative electrode (cf. Fig. 1). The grid is provided with diagonal elements. Case 1 corresponds to the actual samples used to obtain the experimental data.

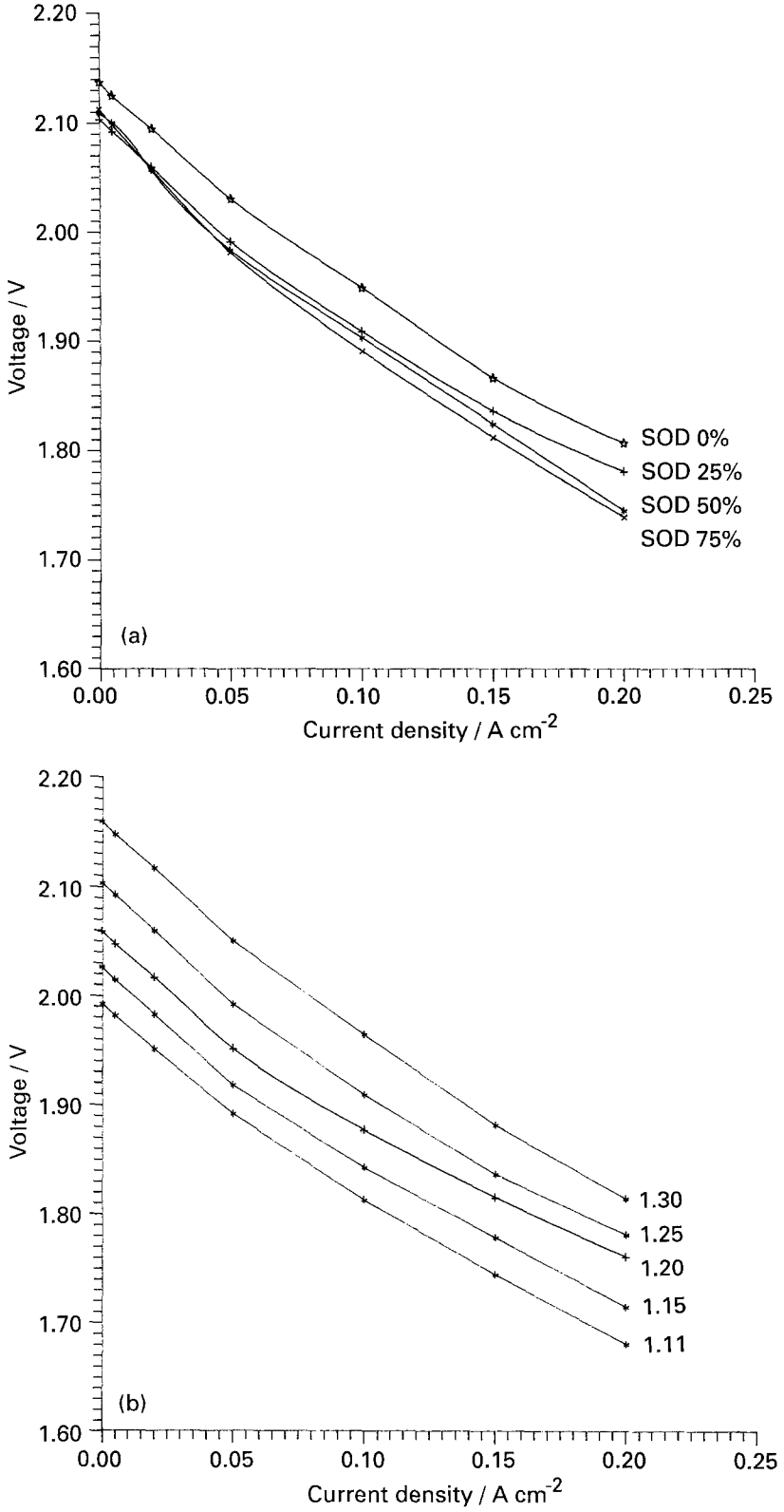

Fig. 3. Polarization plots (iR corrected) for the discrete microcells: (a) as a function of the state of discharge (SOD, indicated on the curves), $d = 1.25\,\mathrm{g\,cm^{-3}}$ and (b) as a function of electrolyte density (numbers indicated in the curves, in $\mathrm{g\,cm^{-3}}$), $SOD = 25\%$.

The theoretical results for the overpotential distribution on the positive and negative electrodes are presented in Figs 4(a) and 4(b), respectively. Equipotential lines show that the maximum ohmic drops are 120 and 96 mV for the positive and negative electrodes, respectively. These values are in good agreement with those presented previously for other electrode systems studied under similar discharge conditions [19, 23], which gives support to the approximations introduced in the present work.

Ohmic losses are smaller in the negative electrode, which is a consequence of the higher conductivity of the negative active material. This is a confirmation that the current flowing through the electrode is conducted by both the grid and the active material, particularly in the case of the negative electrode.

Case 2: This is the same as Case 1 but without diagonal elements in the grid. The maximum ohmic drop is only 5 mV above the value obtained in the previous case.

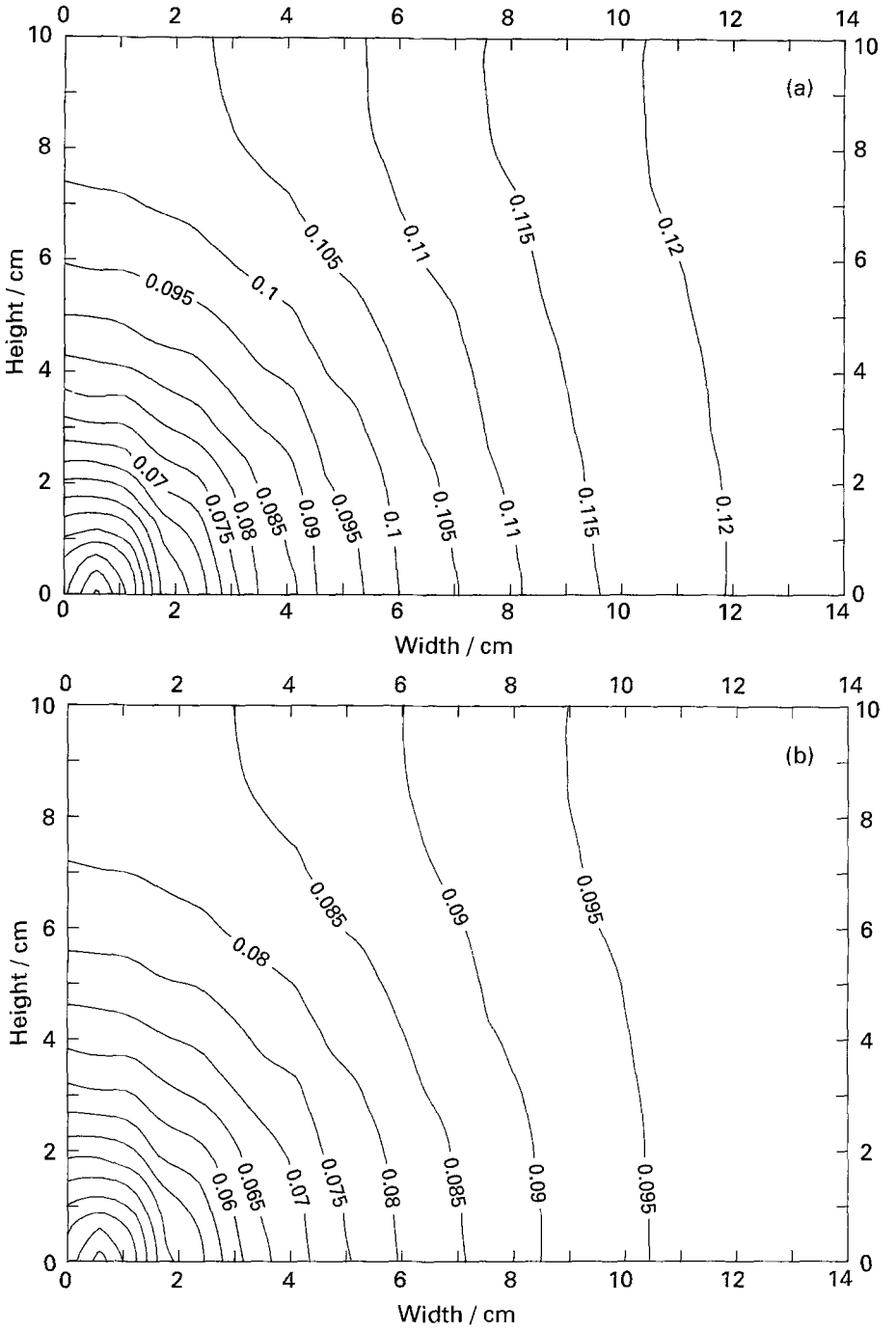

Fig. 4. Equipotential curves for the positive (a) and negative (b) electrodes for initial conditions. The grids are those shown in Fig. 2 and the current density is 300 mA cm^{-2}. Numbers are in volts.

Thus, it may be concluded that the presence of diagonal elements in the grid, placed as shown in Fig. 2, contributes very little toward the reduction of ohmic losses.

Case 3: This is the same as Case 2 but the grid dimensions, while keeping the same total area, are width 11.21 cm and height 11.5 cm. The results for this case are presented in Fig. 5(a). The maximum ohmic loss is 125 mV, that is, essentially the same as in the two previous cases. However, as a consequence of the symmetry of the grid the equipotential lines are also more symmetrical along the electrode surface.

Case 4: This is the same as Case 2 but with a marked asymmetry in the grid dimensions of width 7.225 cm and height 19.4 cm. As shown in Fig. 5(b) this has a strong effect toward increasing ohmic losses.

Case 5: This is the same as Case 3 but with the lug width increased to 1.445 cm. The maximum ohmic loss was reduced only 5 mV, so the effect may be considered very small.

Case 6: Here the situation is similar to Case 1 but the lug is positioned at the upper centre of the plates. The results are presented in Fig. 5(c) and show a dramatic (over 40%) reduction of ohmic losses. This result confirms the conclusions of a previously published mathematical model [19] stressing the importance of the lug position on the homogeneity of the ohmic potential distribution.

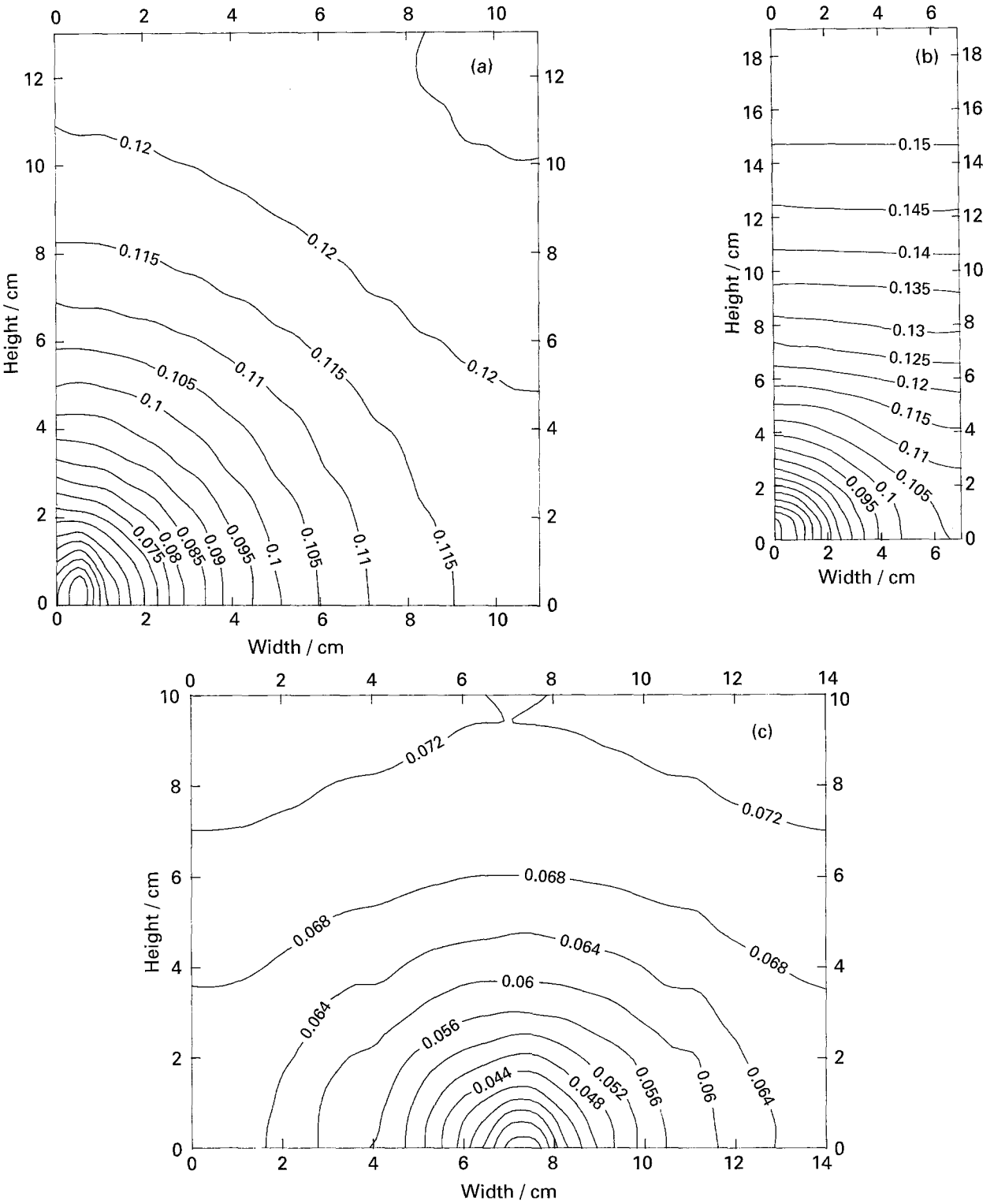

Fig. 5. Equipotential curves for positive electrodes discharging under the initial conditions at 300 mA cm^{-2}. Diagrams (a) to (c) correspond to Cases 3, 4 and 6, respectively (see text). Numbers are in volts.

Figure 6(a) and (b) show examples of the current density distributions corresponding to Cases 1 and 6, respectively. For the other cases the results were qualitatively similar. As expected, current densities are higher near the lug and non-uniform throughout the electrode. This means that a more pronounced consumption of active material should be expected near the lug, at least at the beginning of battery operation.

Regarding electrode design, the results of applying the model of Morimoto *et al.* [23] to Cases 1 to 4 lead to the conclusion that the electrode geometry is very important in determining the extent of ohmic losses. The best geometry is that of a square grid, although some asymmetry is acceptable. The contribution of diagonal elements is not significative enough to warrant their inclusion in grid design. Cases 5 and 6 show that the size of the lug does not

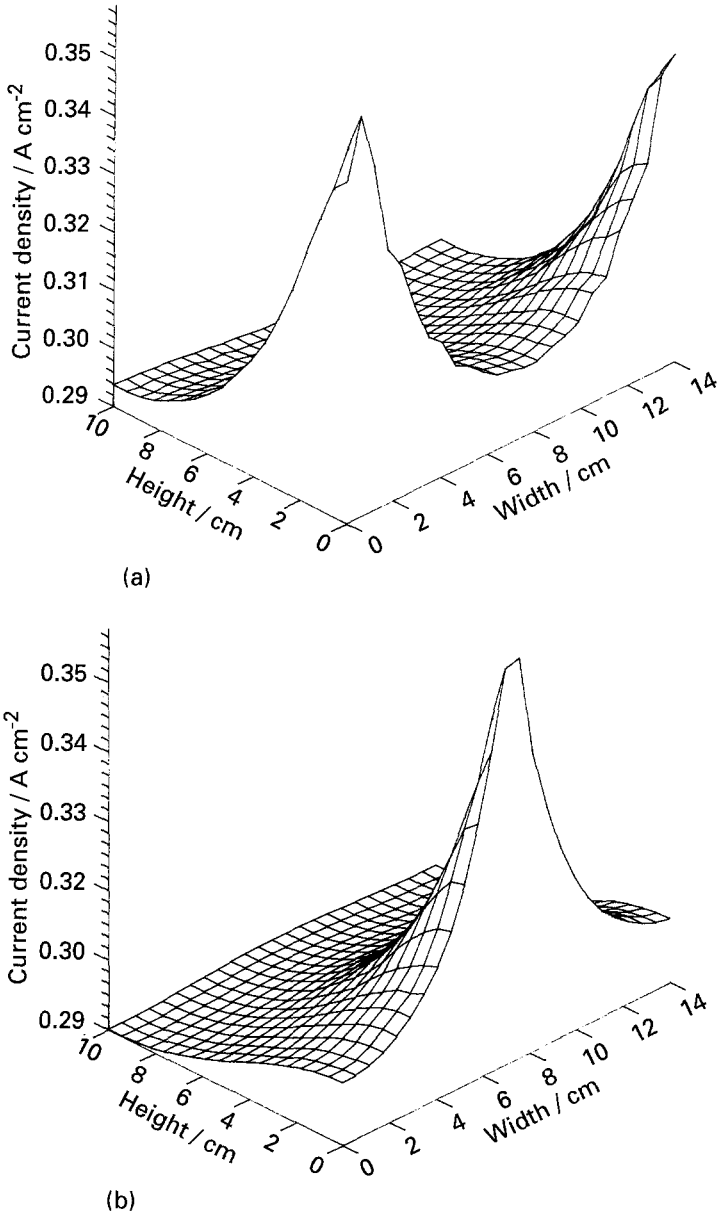

Fig. 6 Current density distributions under the initial conditions at 300 mA cm^{-2} for: (a) Case 1 and (b) Case 6 (see text).

seem to be critical but, on the other hand, its position in the plate should be one of the important aspects to be taken into account in cell design.

It is important to note that most of the above conclusions obtained using Morimoto's model were in agreement with results already presented in the literature [19–22]. The only apparent difference is the observation of the secondary importance of the diagonal elements. However this conclusion is a consequence of the particular grid design employed in the present work. It can be seen in Fig. 2 that the diagonal elements are not electrically connected to the lug, leaving a conductivity gap in a small region where a large iR drop is present in the electrode (Fig. 4).

4.2. *Low discharge currents*

At low discharge currents and for sufficiently long periods of time the behaviour of the battery is determined by the changes in the electrolyte and active materials. During the discharge, water is produced and sulphuric acid consumed which results in a dilution of the electrolyte. Additionally, due to the action of convective forces and/or as a consequence of high current densities flowing at the top of the cells, the electrolyte density varies along the vertical axis. Due to this stratification phenomenon [29] and to the changes in conductivity of the active materials the current density distributions have a strong dependence on discharge time. Thus, theoretical calculations were made as a function of time for a battery discharging at a constant current of 5 mA cm^{-2}, which corresponds to $I_0 = 0.7$ A.

According to the Morimoto model, after calculating the distribution of $J(i,j)$ between the electrodes for the initial conditions (battery fully charged and homogeneously distributed electrolyte at $d = 1.270$ g cm^{-3}) an amount of discharge $Q(i,j)$ is calculated by adding $J(i,j) \times \Delta t$, where Δt is the time increment, to the initial situation. For the new state of discharge a new set of data is entered and new values of potential and current density distribution are determined. This process is repeated until the terminal voltage decreases

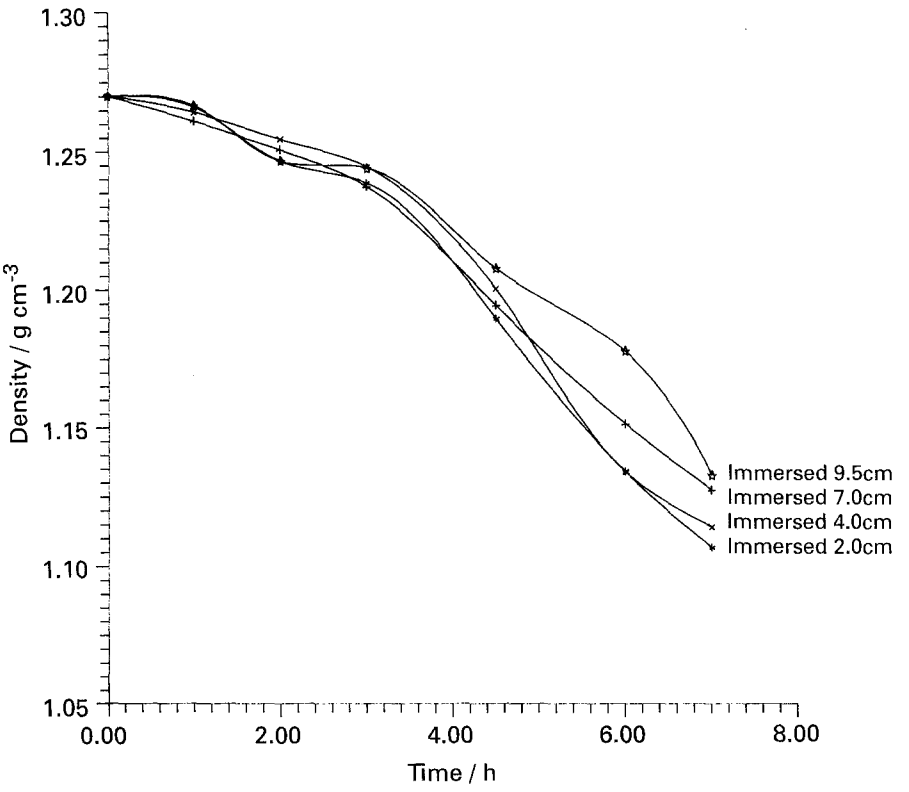

Fig. 7. Electrolyte density as a function of discharge time at various vertical positions along the electrode.

to the cut-off value of 1.75 V. In order to implement this procedure the following parameters are needed:

(i) The electrolyte density at each point. Figure 7 shows experimental results of the variation of electrolyte density with time for different heights. From these curves the values needed in the simulations were obtained by a 4th order polynomial interpolation of density against time data and a 3rd order polynomial interpolation of density against height data.

(ii) The resistance of the active materials at each point. These were calculated by assuming that the conductivity of the active material $S(i,j)$ changes with the state of discharge according to the expression [23]:

$$S(i,j) = S_0(1 - Q(i,j)/Q_T) \qquad (6)$$

where Q_T is the theoretical capacity, calculated from the mass of active material at the given point, and S_0 is the conductivity of the fully charged active material.

(iii) The polarization characteristics of the electrode. Current-potential curves were obtained experimentally and some examples are shown in Fig. 3. As pointed out before these data were obtained for samples in several state of discharge and electrolyte densities. The data necessary for the simulations were interpolated at any current density from the current-potential curves using a 3rd order polynomial. Linear regressions were used to calculate data for any state of discharge and electrolyte density.

In order to obtain the characteristics of the system for different states of discharge the looping time increment in the calculations was set at 1 min.

Figure 8(a) shows the current density distribution at the beginning of discharge ($t = 0$) where there is no stratification of the electrolyte. The current distribution is qualitatively the same as that observed for high current densities. After one hour of discharge at 5 mA cm^{-2} (Fig. 8(b)) there is an increase in the participation of the bottom of the cell and a large decrease of the contribution of the elements at the top. After two hours the middle region of the electrode starts to participate more effectively, reaching a maximum at about 3 h (Fig. 8(c)). For long times this contribution gradually diminishes and becomes negligible at about 5 h (Fig. 8(d)).

These results show qualitative and quantitative differences when compared with those presented for up to 5 h by Morimoto *et al.* [23] for a similar modelling approach of the battery operation under the same current density. Because of the large number of parameters involved, it is difficult to identify the causes for the discrepancies. They could arise as a consequence of several small differences in the materials employed and consequently, in the experimental data, in particular those of the polarization curves for the several states of discharge and electrolyte densities, and those of the stratification of the electrolyte as a function of the electrode height and time.

Figure 9(a) and (b) shows the current distribution profile for 6 and 7 h of battery operation. Here, it is important to note that for these long times of operation the model predicts the existence of negative current densities in some regions of the electrode, which is equivalent to say that in these regions a charging process is taking place.

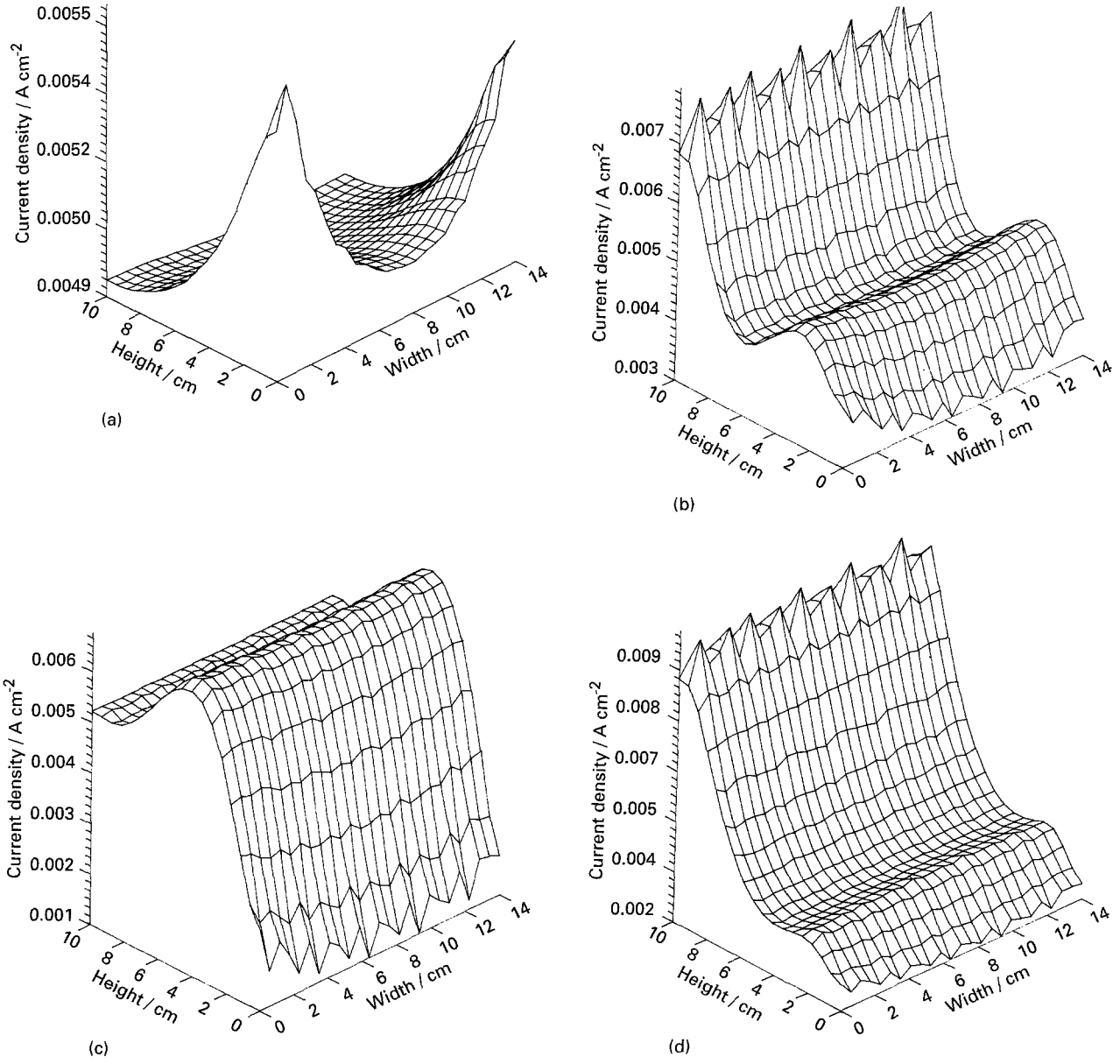

Fig. 8. Current density distributions at 5 mA cm^{-2} as a function of discharge time: (a) 0 h, (b) 1 h, (c) 3 h and (d) 5 h.

It must be pointed out that the values of the charging current densities were calculated from the extrapolation of $[V_p(i,j) - V_n(i,j)]$ versus $J(i,j)$ data obtained for the discharging process. The crucial point is that, for the charging microcells which are in a given state of discharge in contact with the electrolyte in a given density, the program calculates a value of the cell voltage higher than that of the open circuit. This value is then used to calculate the charging current densities using the extrapolated data.

The appearance of charging currents is a consequence of the stratification of the electrolyte which promotes the formation of short-circuited concentration microcells localized along the electrode surface. Thus, other regions of the electrode provide the current that flows through the external load plus the excess current necessary to charge the internal microcells.

The electrolyte density changes along the vertical axis of the cell as a consequence of the action of convective forces and of the uneven distribution of current densities. The convective effects are driven by external forces not controlled by the cell voltage (e.g. gravity) and constitute the major factor responsible for the appearance of the charging currents. The second effect is controlled by the cell voltage and, being self-regulated, does not contribute to the charging phenomenon.

5. Conclusions

The results of applying a resistive grid model to study the current and ohmic overpotential distributions along the surface of lead–acid battery electrodes can be summarized as follows:

(i) It is confirmed that ohmic losses are smaller in the negative than in the positive electrode as a consequence of the higher conductivity of the negative active material.

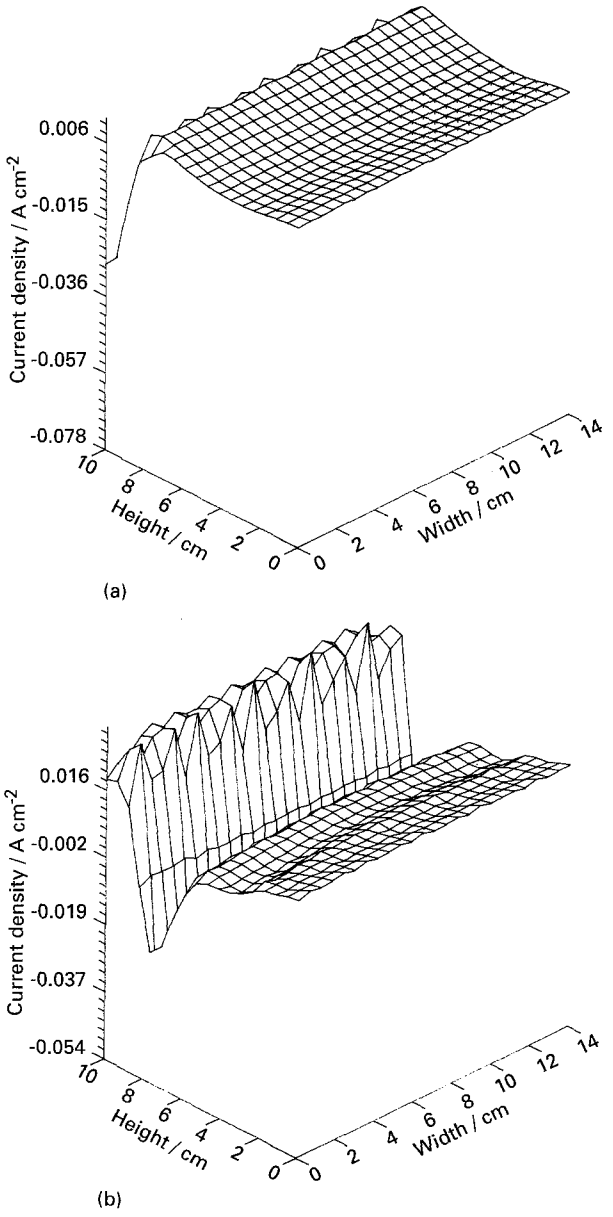

Fig. 9. Same as in Fig. 8 for discharge times: (a) 6 h and (b) 7 h.

(ii) The geometry of the electrode and the position of the lug play an important role in determining the magnitude of ohmic losses. Square grids present the better geometry, while the upper centre of the electrodes is the best position for the lug.

(iii) For a continuous discharge at $5\,mA\,cm^{-2}$ the effect of the stratification of the electrolyte predominates in determining the current density distribution.

(iv) For long discharge times at low currents the results show the existence of short circuited concentration microcells on the electrode surface. Thus, other regions of the electrode must provide an excess current to charge these microcells. The existence of such concentration microcells during the discharge of lead–acid battery have not been predicted in previous work and correspond to one of the most important observations of the present work.

Acknowledgements

The authors thank the Conselho Nacional de Desenvolvimento Científico e Tecnológico (CNPq) and the Financiadorade de Estudos e Projetos (FINEP), Brazil, for financial support.

References

[1] J. S. Newman and C. W. Tobias, *J. Electrochem. Soc.* **109** (1962) 1183.
[2] J. S. Dunning, D. N. Bennion and J. S. Newman, *ibid.* **118** (1971) 1251.
[3] D. Simonsson, *ibid.* **120** (1973) 151.
[4] D. Simonsson, *J. Appl. Electrochem.* **3** (1973) 261.
[5] *Idem, ibid.* **4** (1974) 109.
[6] K. Micka and I. Rousar, *Electrochim. Acta* **18** (1973) 629.
[7] *Idem, ibid.* **19** (1974) 499.
[8] *Idem, Coll. Czechoslovak Chem. Comm.* **40** (1975) 921.
[9] *Idem, Electrochim. Acta* **21** (1976) 599.
[10] J. Newman and J. Tiedemann, *AIChE J.* **21** (1976) 25.
[11] W. H. Tiedeman and J. Newman, *in* 'Battery Design and Optimization', (edited by S. Gross), The Electrochemical Society Proceedings Series, Princeton, NJ (1979) p. 23.
[12] W. S. Sunu, *in* 'Electrochemical Cell Design', (edited by R. E. White), Plenum Press, New York (1984) p. 357.
[13] H. Gu, T. V. Nguyen and R. E. White, *J. Electrochem. Soc.* **134** (1987) 2953.
[14] E. C. Dimpault-Darcy, T. V. Nguyen and R. E. White, *ibid.* **135** (1988) 278.
[15] P. Ekdunge and D. Simonsson, *J. Appl. Electrochem.* **19** (1989) 136.
[16] W. Tiedeman, J. Newman and F. DeSus, *in* 'Power Sources 6', (edited by D. H. Collins), Academic Press, New York (1977).
[17] L. E. Vaaler, *J. Appl. Electrochem.* **9** (1979) 21.
[18] W. H. Tiedeman and J. Newman, *op. cit.* [11], p. 39.
[19] W. G. Sunu and B. W. Burrows, *J. Electrochem. Soc.* **129** (1982) 688.
[20] L. E. Vaaler, E. W. Brooman and H. A. Fugitti, *J. Appl. Electrochem.* **12** (1982) 721.
[21] H. Gu, *J. Electrochem. Soc.* **130** (1983) 1459.
[22] W. G. Sunu and B. W. Burrows, *ibid.* **131** (1984) 1.
[23] Y. Morimoto, Y. Ohya, K. Abe, T. Yoshida and H. Morimoto, *ibid.* **135** (1988) 293.
[24] H. Gu, *J. Appl. Electrochem.* **19** (1989) 505.
[25] B. Carnahan, H. A. Luther and J.O. Wilkes, 'Applied Numerical Methods', John Wiley & Sons, New York (1969).
[26] M. J. D. Powell, *in* 'Numerical Methods for Nonlinear Equations', (edited by P. Rabinowitz), Gordon and Breach Science Publishers, London (1970) p. 87.
[27] C. G. Broyden, *Math. Computation* **21** (1967) 368.
[28] S. U. Falk and A. J. Salkind, *in* 'Alkaline Storage Batteries', John Wiley & Sons, New York (1969) p. 253.
[29] W. G. Sunu and B. W. Burrows, *J. Electrochem. Soc.* **128** (1981) 1405.